DOI:
10.1038/s42005-019-0254-1

Evening out the spin and charge parity to increase T_c in Sr_2RuO_4

Swagata Acharya[1*], Dimitar Pashov[1], Cédric Weber[1],
Hyowon Park[2,3], Lorenzo Sponza[4], Mark van Schilfgaarde[1]

[1]King's College London, The Strand, WC2R 2LS London, UK,
[2]Department of Physics, University of Illinois at Chicago, Chicago, Illinois 60607, USA,
[3]Materials Science Division, Argonne National Laboratory, Argonne, Illinois, 60439, USA,
[4]LEM UMR 104, ONERA-CNRS, F-92322, Châtillon, France

[*]E-mail: swagata.acharya@kcl.ac.uk

Unconventional superconductivity in Sr_2RuO_4 has been intensively studied for decades. The origin and nature of the pairing continues to be widely debated, in particular, the possibility of a triplet origin of Cooper pairs. However, its complexity, with multiple low-energy scales involving subtle interplay among spin, charge and orbital degrees of freedom, calls for advanced theoretical approaches which treat on equal footing all electronic effects. Here we develop a novel approach, a detailed *ab initio* theory, coupling quasiparticle self-consistent *GW* approximation with dynamical mean field theory (DMFT), including both local and non-local correlations. We report that the superconducting instability has multiple triplet and singlet components. In the unstrained case the triplet eigenvalues are larger than the singlets. Under uniaxial strain, the triplet eigenvalues drop rapidly and the singlet components increase. This is concomitant with our observation of spin and charge fluctu-

ations shifting closer to wave-vectors favoring singlet pairing in the Brillouin zone. We identify a complex mechanism where charge fluctuations and spin fluctuations co-operate in the even-parity channel under strain leading to increment in T_c, thus proposing a novel mechanism for pushing the frontier of T_c in unconventional 'triplet' superconductors.

The nature and origin of superconducting pairing in unconventional superconductor Sr_2RuO_4 (SRO) has been one of the most debated topics [6] in materials research over last two decades. The superconductivity in SRO has signatures supporting a spin-triplet origin, which raises the possibility that it can sustain Majorana states conducive for topological quantum computing [4], making it an active field of research and a case to study with advanced theoretical and experimental methods. A series of recent experimental findings, including strain dependent enhancement in T_c [11], H_{c2} anomaly and the state-of-the are O^{17} NMR [48] observations have challenged the existing beliefs and demands a fresh look into the enigmatic problem of superconductivity in SRO.

SRO single crystals were first shown to exhibit superconductivity below 1.5 K in 1994 [5]. Within few years of its discovery it was established that the superconductivity is highly sensitive to disorder [3]. Ever since efforts have been made to understand the mechanism of pairing and drive the T_c higher. The superconducting transition temperature, T_c, has been observed to increase to 3 K in eutectic crystals of SRO, in the vicinity of Ru inclusions [7, 8, 9]. While enhancement of T_c was traditionally associated with a reduced volume fraction, a recent series of experiments [10, 11] on bulk single crystals of SRO subject to uniaxial strain, show an increase to 3.4 K for compressive strain in the [100] direction, which we denote as ϵ_x. These apparently dissimilar studies hint towards a more common underlying mechanism for enhancement of T_c, since Ru inclusions induce local stresses which include uniaxial strain. In the tensile experiments T_c can be controlled by varying ϵ_x. It reaches a maximum value at ϵ_x=0.6% [11], beyond

which it falls rapidly. In what follows we will denote ϵ_x=0.6% as ϵ_x^*.

These observations challenge the established belief that SRO is a spin-triplet (odd-parity) superconductor. Under strain, the tetragonal symmetry of the compound is lost, and it is no longer possible to find a triplet order parameter from two degenerate components, such as the usual $p_x + ip_y$ or $d_{xz} + id_{yz}$. This raises the possibility for alternative mechanisms that could be responsible for pairing under strain.

The effect of strain on the Fermi surface has been studied with density functional theory (DFT) [11], and complementary minimal model Hamiltonian approaches [12, 13], which identified a change in Fermi surface topology. In particular, a Van Hove singularity [11] approaches the Fermi level, with a concomitant increase in charge carriers, which has been suggested as a possible mechanism for the increment in T_c [14] under strain. Such a picture identifies an important property resulting from strain, but it is not sufficient to explain the enhancement of T_c. In particular, the multi-orbital nature of the spin and charge fluctuations and many-body correlations are shown to be important in SRO [15, 16, 17, 18]. Novel electron correlations originating from competition between non-local Coulomb repulsion and the large Hund's coupling [19, 15, 20] are also significant.

It is a formidable challenge to adequately describe the single- and two-particle responses needed for insights into the origin and nature of superconductivity in SRO. As we show here, an accurate theoretical formulation, that includes both local and non-local correlation effects in space, momentum and time and for all relevant degrees of freedom, is essential. Recently, a significant advance has been achieved by combining the quasi-particle self consistent *GW* (QS*GW*) approximation, with dynamical mean field theory (DMFT) [21, 22]. Merging of these two state-of-the-art methods captures the effect of both strong local dynamic spin fluctuations (captured well in DMFT), and non-local dynamic correlation [23] effects (captured by QS*GW*), relying on neither model hamiltonians, nor on DFT, and avoiding the concomitant limitations

they each carry. Also, nonlocal spin, charge and pairing susceptibilities can also be obtained from vertices computed from the local two-particle Green's sampled by DMFT and bubble diagrams, via the solutions of Bethe Salpeter equations in respective channels. The full numerical implementation is discussed in Pashov et. al. [24] and codes are available on the open source electron structure suite Questaal [25].

Here we apply this new methodology to SRO, studying the pristine compound and also the effect of strain. Through the vertices and susceptibilities we can identify what drives superconductivity, and also what causes the non-monotonic dependence of T_c on strain. The pairing instability has multiple singlet and triplet components; nodal structure in the singlet channel and nodeless odd-frequency structure in the triplet channel. We find that the pairing is favored by even parity couplings in both spin and charge channels as ϵ_x approaches ϵ_x^* from below, while for $\epsilon_x > \epsilon_x^*$ incoherent spin fluctuations suppress the superconducting order. Our observations are in remarkable agreement with recent neutron scattering experiments [26].

Evolution of Fermi surface topology under strain: Fermi surfaces in the basal plane are shown in Fig. 1. The critical change in topology on the line connecting (0,0) and (0,π) (points Γ and M) occurs at ϵ_x=0.6%, in excellent agreement with ϵ_x^*. This is the strain where one Van-Hove singularity crosses E_F (see SM), as was noted in a prior DFT study; though in DFT it does so at a much larger ϵ_x (see Fig. 1). The Fermi surface generated by QS*GW* closely matches recent high-resolution bulk Fermi surface observed in quantum oscillation studies [27] angle-resolved photo-emission spectroscopy [28, 29]; indeed they can only be easily distinguished at at higher resolution (as shown in SM, Fig. 1). That QS*GW* simultaneously yields the topology change close to the observed ϵ_x^*, and can reproduce fine details of the ARPES Fermi surface, is a reflection of its superior ability to generate good effective noninteracting Hamiltonians.

Spin fluctuations: incommensurability and coherence: Spin (χ^m) and charge (χ^d) susceptibilities are computed from momentum dependent Bethe-Salpeter equations 1 in magnetic (spin)

and density (charge) channels.

$$\chi^{m(d)}_{\substack{\alpha_1,\alpha_2\\ \alpha_3,\alpha_4}}(i\nu, i\nu')_{\mathbf{q},i\omega} = [(\chi^0)^{-1}_{\mathbf{q},i\omega} - \Gamma^{irr,m(d)}_{loc}]^{-1}_{\substack{\alpha_1,\alpha_2\\ \alpha_3,\alpha_4}}(i\nu, i\nu')_{\mathbf{q},i\omega}. \quad (1)$$

χ^0 is the non-local (k-dependent) polarization bubble computed from single-particle QS*GW* Green's functions dressed by DMFT and Γ is the local irreducible two-particle vertex functions computed in magnetic and density channels. Γ is a function of two fermionic frequencies ν and ν' and the bosonic frequency ω. The susceptibilities $\chi^{m(d)}(\mathbf{q}, i\omega)$ are computed by closing $\chi^{m(d)}_{\substack{\alpha_1,\alpha_2\\ \alpha_1,\alpha_2}}(i\nu, i\nu')_{\mathbf{q},i\omega}$ with spin or charge bare vertex γ (γ=1/2 for spin and γ=1 for charge) and summing over frequencies ($i\nu$,$i\nu'$) and orbitals ($\alpha_{1,2}$) (see SM for derivations).

$$\chi^{m(d)}(\mathbf{q}, i\omega) = 2\gamma^2 \sum_{i\nu,i\nu'} \sum_{\alpha_1\alpha_2} \chi^{m(d)}_{\substack{\alpha_1,\alpha_2\\ \alpha_1,\alpha_2}}(i\nu, i\nu')_{\mathbf{q},i\omega}. \quad (2)$$

We focus first on the Γ-X line of the Brillouin zone, where peaks appear in inelastic neutron scattering measurements [30, 31, 32] at the incommensurate vector q^{IC}=$(0.3, 0.3, 0)$ (in units $2\pi/a$) which a maximum in frequency near ω=10 meV. Using DMFT, we compute $\chi^m(\mathbf{q}, \omega)$ by obtaining the local two-particle vertex in the spin channel and solving the Bethe-Salpeter equation [33], for varying amounts of strain. Consider first the unstrained case, where measurements are available. Fig. 2 shows $\chi^m(q, \omega)$ on the Γ-X line and in planes q_z = 0, 1/4, and 1/2 (in units of $2\pi/c$). The peak noted above [q^{IC}=$(0.3, 0.3, 0)$, ω=10 meV] is nearly independent of q_z, and moreover it disperses all the way up to 80 meV. All of these findings are in excellent agreement with experimental observations [34]. We also find significant spin fluctuations at the ferromagnetic (FM) vector q=$(0, 0, 0)$ (also seen in very recent neutron measurements[26]) and almost no intensity at the antiferromagnetic nesting vector (1/2,1/2,0). The FM signal is important, because of its implications for superconductivity [26] and whether the pairing is of triplet or singlet character. We find that the intensity of $\chi^m(q$=$0)$ is $\sim$1/5 of the dominant IC peak when spin-orbit coupling (SOC) is suppressed. SOC lifts band degeneracies at high symmetry points

and reduces this ratio slightly, to ∼1/7. Thus χ^m seems to be dominated by fluctuations at $q^{\rm IC}$. Such spin fluctuations should favour pairing mainly in the spin singlet channel, absent other channels to provide extra glue for a triplet pairing. However, the continuum of spin excitations elsewhere in the Brillouin zone also contribute to the glue.

As strain is applied $\mathrm{Im}\chi^m(q,\omega)$ becomes sharper and more coherent, reaching a maximum coherence at ϵ_x=ϵ_x^*: the peak intensity remains at $q^{\rm IC}$ but nearly doubles in strength and shifts to slightly smaller ω. Also $\mathrm{Im}\chi^m$ loses its two-dimensional character: the q_z dependence is significant and the dominant peak is most intense at $1/4$. For still larger ϵ_x, coherence begins to be lost. At ϵ_x=1.2% the IC peak $(0.3, 0.3, q_z)$ survives but χ^m becomes incoherent and diffused over a range of q both in the plane and out of it, with another peak appearing near $(0.15, 0.15, 0)$. In short, for ϵ_x>ϵ_x^*, two prominent changes are observed: incommensurate but nearly ferromagnetic excitations at $(0.15, 0.15, 0)$ and commensurate gapped antiferromagnetic spin excitations at $(1/2, 1/2, a/2c)$.

Charge susceptibilities and commensurability: The evolution of the spin and charge susceptibilities are instructive to understand the changes in the gap symmetries under strain and their underlying even- or odd-parity characters. We find that the real part of the charge susceptibilities in the static limit $\chi^d(q, \omega\rightarrow0)$, has strong peaks at ∼(0.2,0.2,0), in the vicinity of the ferromagnetic vector, and also near the anti-ferromagnetic vector (1/2,1/2,0) (Fig. 3). Raghu et al. discuss a possible route to superconductivity through charge fluctuations originating from the quasi one-dimensional bands d_{xz} and d_{yz} [35]. Their analysis relies on the quasi one-dimensional character of these states. Our *ab initio* calculation partially supports this picture. However, we also observe nearly comparable multi-orbital charge fluctuations, both intra and inter-orbital in nature, in all active bands (Fig 3). *Inter*-orbital charge fluctuations originating from d_{xz} and d_{yz} and the two-dimensional d_{xy} are comparable to, or even larger than the intra-orbital contributions.

In the unstrained case, nearly uniform long-wavelength coherent charge fluctuations support a triplet pairing channel mainly through multi-orbital charge fluctuations. There is a significant peak in χ^d at small q, near (0.2,0.2,0). However, there is another broad peak near (1/2,1/2,0). Under strain, the latter peak becomes more coherent and larger, while the former decays, and at the critical strain ϵ_x^* only the latter peak remains. Also χ^m and χ^d become increasingly coherent close to a vector that favors singlet pairing. This is strikingly different from the unstrained scenario where both spin and charge fluctuations have favourable triplet components as well. For $\epsilon_x > \epsilon_x^*$, χ^d at (1/2,1/2,0) becomes large. Simultaneous shifts in spin fluctuation weight towards more commensurate lower q (larger wavelength) leaves $\chi^m(q^{\rm IC})$ incoherent, which in turn weakens the ability to form Cooper pairs.

Superconducting pairing: nodal character and dimensionality: The superconducting pairing susceptibility χ^{p-p} is computed by dressing the non-local pairing polarization bubble $\chi^{0,p-p}(\mathbf{k}, i\nu)$ with the pairing vertex $\Gamma^{irr,p-p}$ using the Bethe-Salpeter equation in the particle-particle channel.

$$\chi^{p-p} = \chi^{0,p-p} \cdot [\mathbf{1} + \Gamma^{irr,p-p} \cdot \chi^{0,p-p}]^{-1} \tag{3}$$

$\Gamma^{irr,p-p}$ in the singlet (s) and triplet (t) channels are obtained from the magnetic (spin) and density (charge) particle-hole reducible vertices by

$$\begin{aligned}\Gamma^{irr,p-p,s}_{\substack{\alpha_2,\alpha_4\\ \alpha_1,\alpha_3}}(\mathbf{k}, i\nu, \mathbf{k}', i\nu') &= \Gamma^{f-irr}_{\substack{\alpha_2,\alpha_4\\ \alpha_1,\alpha_3}}(i\nu, i\nu') + \frac{1}{2}[\frac{3}{2}\widetilde{\Gamma}^{p-h,(m)} - \frac{1}{2}\widetilde{\Gamma}^{p-h,(d)}]^{\alpha_2,\alpha_3}_{\alpha_1,\alpha_4}(i\nu, -i\nu')_{\mathbf{k}'-\mathbf{k}, i\nu'-i\nu} \\ &\quad + \frac{1}{2}[\frac{3}{2}\widetilde{\Gamma}^{p-h,(m)} - \frac{1}{2}\widetilde{\Gamma}^{p-h,(d)}]^{\alpha_4,\alpha_3}_{\alpha_1,\alpha_2}(i\nu, i\nu')_{-\mathbf{k}'-\mathbf{k}, -i\nu'-i\nu}\end{aligned} \tag{4}$$

$$\begin{aligned}\Gamma^{irr,p-p,t}_{\substack{\alpha_2,\alpha_4\\ \alpha_1,\alpha_3}}(\mathbf{k}, i\nu, \mathbf{k}', i\nu') &= \Gamma^{f-irr}_{\substack{\alpha_2,\alpha_4\\ \alpha_1,\alpha_3}}(i\nu, i\nu') - \frac{1}{2}[\frac{1}{2}\widetilde{\Gamma}^{p-h,(m)} + \frac{1}{2}\widetilde{\Gamma}^{p-h,(d)}]^{\alpha_2,\alpha_3}_{\alpha_1,\alpha_4}(i\nu, -i\nu')_{\mathbf{k}'-\mathbf{k}, i\nu'-i\nu} \\ &+ \frac{1}{2}[\frac{1}{2}\widetilde{\Gamma}^{p-h,(m)} + \frac{1}{2}\widetilde{\Gamma}^{p-h,(d)}]^{\alpha_4,\alpha_3}_{\alpha_1,\alpha_2}(i\nu, i\nu')_{-\mathbf{k}'-\mathbf{k}, -i\nu'-i\nu}\end{aligned} \tag{5}$$

$\Delta_{(\alpha_1,\alpha_2),(\alpha_3,\alpha_4)}$	$\hat{S}$	$\hat{O}$	$\hat{T}$	$\hat{P}$	pairing functions	irreps
$d_{(xy,xy),(xy,xy)}$	-1	1	1	1	$d_{x^2-y^2}$	B_{1g}
$d_{(xz,xz),(yz,yz)}$	-1	1	1	1	$S^{\pm}$	A_{1g}
$d_{(xz,xz),(yz,yz)}$	-1	1	1	1	$d_{x^2-y^2}$	B_{1g}
$d_{(xy,xy),(xy,xy)}$	1	1	-1	1	$S^{\pm}$	A_{1g}
$d_{(xz,xz),(yz,yz)}$	1	1	-1	1	$S^{\pm}$	A_{1g}
$d_{(xz,xz),(yz,yz)}$	1	1	-1	1	$d_{x^2-y^2}$	B_{1g}

Table 1: Characterization of different singlet and triplet gap instabilities in terms of D_{4h} irreducible representation. Also shown is how these different gap instabilities transform under spin exchange $\hat{S}$, orbital exchange $\hat{O}$, time exchange $\hat{T}$ and parity $\hat{P}$ operators.

Finally, χ^{p-p} can be represented in terms of eigenvalues λ and eigenfunctions ϕ^{λ} of the Hermitian particle-particle pairing matrix (see the SM for detailed derivation).

$$\chi^{p-p}(k,k') = \sum_{\lambda} \frac{1}{1-\lambda} \cdot (\sqrt{\chi^{0,p-p}(k)} \cdot \phi^{\lambda}(k)) \cdot (\sqrt{\chi^{0,p-p}(k')} \cdot \phi^{\lambda}(k')) \tag{6}$$

The pairing susceptibility diverges when the leading eigenvalue approaches unity. The corresponding eigenfunction represents the momentum structure of χ^{p-p}. However, unlike hole doped cuprates or doped single-band Hubbard model [36], the unconventional superconductivity in SRO is multi-orbital in nature with a close packed eigenvalue spectrum, which warrants more detailed investigation of the different eigenfunctions.

As is apparent from Eqns. 4, 5 at what wave vector spin and charge fluctuations are strong is of central importance to the kind of superconducting pairing symmetry they can form. If superconductivity is driven by fluctuations near the ferromagnetic point (0,0,0), the spin part of the Cooper pair is symmetric and the superconductivity should have triplet symmetry. If, on the other hand if the fluctuations (spin or charge) are more proximate to $(1/2, 1/2, q_z)$, the symmetry is more likely to be singlet.

Before presenting QSGW+DMFT+BSE results for the pairing susceptibility, we summarize a few key findings in the past year which have dramatically altered (and obfuscated) the consen-

sus for origins of superconductivity in SRO. New experiments have sown considerable doubt that the gap function Δ is a chiral p wave. Much of the basis for the long held consensus that SRO is a spin-triplet superconductor, with chiral order parameter $p_x \pm i p_y$, was derived from observation that the Knight shift did not change through the superconducting transition [38]. Kerr effect [39] and muon spin rotation [40] measurements also provide evidence for broken time reversal symmetry. Recently, however [48], it was found that the Knight shift does change through T_c (the original measurement was an artifact of sample heating). Also recent measurements of thermal conductivity present evidence for vertical line nodes in Δ [50], making a case for the H_{c2} anomaly in SRO. Such nodes preclude the possibility of a p wave order parameter, at least one driven by symmetry. In a recent specific heat study, under angular variation of magnetic field at very low temperatures, Kittaka et al. [51] found horizontal line nodes in the gap structure.

Singlet channel: QSGW+DMFT+BSE calculations yield three dominant eigenvalues in the superconducting gap instabilities. For ϵ_x=0 we find that all eigenvalues are degenerate within numerical precision. The corresponding eigenfunctions are shown in Fig. 4. They all change sign; thus the gap instabilities have nodes. In the $d_{xy,xy}$ channel, the gap function is a d-wave, approximately $\cos k_x - \cos k_y$, with a D_{4h}-B_{1g} irreducible representation. The other two eigenfunctions are respectively $\cos k_x$ and $\cos k_y$ in the $d_{xz,xz}$ and $d_{yz,yz}$ channels. In particular, when a Cooper pair forms with the two quasiparticles belonging to different orbitals, it is possible to get an in-phase extended s-wave symmetry with a $d_{xz,yz}$ gap function $\cos k_x + \cos k_y$ with irreducible representation A_{1g}. Cooper pairs may also form with the quasi-particles out of phase, leading to a $d_{xz,yz}$ gap function with d-wave $\cos k_x - \cos k_y$ symmetry.

Triplet channel: A very different story emerges. We find three nodeless odd-frequency gap instabilities as shown in Fig. 4. In the $d_{xz,xz}$ and $d_{yz,yz}$ channels we observe instabilities of the form $\delta_0 + \cos k_x$ and $\delta_0 + \cos k_y$, leading to the possibility of an extended nodeless s-wave $2\delta_0 +$

$\cos k_x + \cos k_y$ gap structure with A_{1g} irreducible representation in the $d_{xz,yz}$ basis. The out of phase coupling between these two quasi-particles will lead to B_{1g} nodeless d-wave gap structure. We also observe an extended s-wave gap function in the $d_{xy,xy}$ channel. However, additionally we find a doubly-degenerate set of eigenvalues in an off-diagonal $d_{xz,xy}$,$d_{yz,xy}$ channel.

On the Nature of Δ in the unstrained case: Our calculations for Δ are performed in the normal phase of SRO, probing all possible particle-particle instabilities that could precipitate formation of a superconducting gap. They do not describe the superconducting state itself, and do not include possibility of spontaneously breaking time reversal symmetry (TRS). To properly resolve the character of the gap function, a full description of the ordered state is needed [37]. These capabilities we have not yet developed. Nevertheless, the eigenvalues calculated in the normal phase are robust: what is dominant in the orbital basis should remain so in the basis of eigenstates. Thus these instabilities show what states are available to form order parameters prescribed in earlier theoretical works, notably by Raghu et al. [35], Scaffidi et al. [53] and Mackenzie et al. [6]. Such an order parameter can result in a nodeless gap structure which can also lead to TRS breaking and chiral superconductivity. Also, two-component odd-frequency gap functions can lead to observed Kerr rotation in SRO [54]. Also our observation of nodal gap instabilities is consistent with nodal gap structures reported from several measurements and previous theoretical studies based on model Hamiltonians and first principles [41, 42, 43, 44, 45, 46, 47, 52] .

Table shows how different gap structures transform under spin exchange $\hat{S}$, orbital exchange $\hat{O}$, time exchange $\hat{T}$ and parity $\hat{P}$ operators. This allows us to characterize their irreducible representations in terms of D_{4h} lattice symmetry, while noting that under uniaxial strain considered below, this symmetry reduces to D_{2h} and properties relying on 4-fold rotational symmetry no longer apply. Comparing singlet and triplet channels at fixed temperature, the triplet eigenvalues are nearly two times larger than singlet eigenvalues (see Fig. 4), suggesting

variants	λ_s^f	λ_t^f	λ_s^{-c}	λ_t^{-c}
ϵ_x=0	0.006	0.011	0.005	0.014
$\epsilon_x > 0$	0.011	0.007	0.014	0.032

Table 2: The leading singlet and triplet eigenvalues computed using both spin and charge vertex functions λ_s^f, λ_t^f, and by suppressing the charge vertex functions λ_s^{-c}, λ_t^{-c}.

that even while the triplet is dominant, the singlet can contribute significantly to Cooper pair formation (in absence of strain).

Spin-charge co-operation in singlet channel under strain: The relative strengths of singlet and triplet channels reverse under strain. We find that the eigenvalues in the triplet channel decrease rapidly, while the singlet eigenvalues increase (see Fig. 4). Additionally, we find that the triplet eigenvalues are weakly dependent on temperature at this critical ϵ_x^* while the singlet eigenvalues strongly increase with lowering T. The singlet eigenvalues begin to overtake the triplet eigenvalues, suggesting a suppression of the triplet superconducting instability for $\epsilon_x>0$. This is fully consistent with the susceptibility calculations, which suggest that under strain both spin and charge fluctuations becomes more intense close to singlet vectors, and far from triplet $q = 0$. This transition was already conjectured in the original work of Steppke et al [11], based in an interpretation of H_{c2}.

To address the issue conclusively we compute the eigenvalues with and without the charge vertex functions. In the full calculation, we observe that triplet eigenvalues are larger than the singlet eigenvalues at ϵ_x=0. Redoing the calculation suppressing the charge vertex, we find that at ϵ_x=0 triplet eigenvalues remain larger than the singlet eigenvalues. However, $\epsilon_x>0$, suppressing the charge vertex causes triplet eigenvalues to become larger than the singlet eigenvalues, reversing the relative importance of the two. This is a strong indication that both spin and charge vertex functions co-operate under strain in the singlet channel. In Table 2 we show the eigenvalues with and without the charge vertex to quantify this argument.

Conclusion: multiple singlet and triplet superconducting instabilities are observed in SRO. A purely spin triplet superconductivity needs sufficient coherent and low energy spin fluctuation glue near ferromagnetic vector q=0. However, our results show that the dominant spin fluctuations are at $(0.3, 0.3, q_z)$ which is closer to the singlet-pairing vector, combined with the smaller peak at the quasi-ferromagnetic 'triplet' vector. Multi-orbital charge correlations also play a central role in Sr_2RuO_4: they provide additional glue both at low-q and $(0.5, 0.5, q_z)$ through strong intra- and inter-orbital fluctuations. Together, they lead to multiple triplet and singlet Cooper pair instabilities, with triplet eigenvalues exceeding singlet in the absence of strain.

When strain is applied the dominant character of Cooper pair instability changes. $\chi^m(q{=}0.3, 0.3, q_z)$ becomes more coherent up to a critical strain ϵ_x^*. Simultaneously the spectral weight under the low-q charge peak gets fully transferred to a more coherent quasi-anti-ferromagnetic vector $(0.5, 0.5, q_z)$. Together they suggest, spin and charge co-operate to sustain an even parity pairing channel which maximize T_c at ϵ_x^*. For $\epsilon_x{>}\epsilon_x^*$, the spin fluctuation weight drifts toward larger wavelength, more uniform quasi-ferromagnetic vectors and charge fluctuates more strongly at the quasi-anti-ferromagnetic vector. This emergent spin incoherence and spin-charge separation, split by quasi-ferromagnetic spin fluctuation peak and quasi-anti-ferromagnetic charge fluctuation peak, is not conducive for sustaining the even-parity superconductivity and hence lowers and suppresses T_c. Our observations suggest that the pathway to maximize superconductivity in Sr_2RuO_4 would be to cause spin and charge fluctuations to act in symphony in an even parity channel.

Acknowledgments

Authors acknowledge F. Baumberger for sharing with us the raw ARPES data for Fermi surfaces. SA acknowledges discussions with James Annett, Martin Gradhand and Astrid Romer. This work was supported by the Simons Many-Electron Collaboration, and EPSRC (grants

EP/M011631/1 and EP/M011038/1). For computational resources, we were supported by the ARCHER UK National Supercomputing Service, UK Materials and Molecular Modeling Hub for computational resources, (EPSRC grant EP/P020194/1) and computing resources provided STFC Scientific Computing Department's SCARF cluster and PRACE supercomputing facility.

Method

We use a recently developed quasi-particle self consistent *GW* + dynamical mean field theory (QS*GW*+DMFT) [21, 22], as implemented in the all-electron Questaal package [25]. Paramagnetic DMFT is combined with nonmagnetic QS*GW* via local projectors of the Ru $4d$ states on the Ru augmentation spheres to form the correlated subspace. We carried out the QS*GW* calculations in the tetragonal and strained phases of Sr_2RuO_4 with space group 139/I4mmm. DMFT provides a non-perturbative treatment of the local spin and charge fluctuations. We use an exact hybridization expansion solver, namely the continuous time Monte Carlo (CTQMC) [55], to solve the Anderson impurity problem.

The one-body part of QS*GW* is performed on a $16\times16\times16$ k-mesh and charge has been converged up to 10^{-6} accuracy, while the (relatively smooth) many-body static self-energy $\Sigma^0(\mathbf{k})$ is constructed on a $8\times8\times8$ k-mesh from the dynamical GW $\Sigma(\mathbf{k},\omega)$. $\Sigma^0(\mathbf{k})$ is iterated until convergence (RMS change in $\Sigma^0<10^{-5}$ Ry). U=4.5 eV and J=1.0 eV [56] were used as correlation parameters for DMFT. The DMFT for the dynamical self energy is iterated, and converges in ≈ 20 iterations. Calculations for the single particle response functions are performed with 10^9 QMC steps per core and the statistics is averaged over 64 cores. The two particle Green's functions are sampled over a larger number of cores (40000-50000) to improve the statistical error bars. We sample the local two-particle Green's functions with CTQMC for all the correlated orbitals and compute the local polarization bubble to solve the inverse Bethe-Salpeter equation (BSE) for the local irreducible vertex. Finally, we compute the non-local polarization bubble

$G(\mathbf{k},\omega)G(\mathbf{k}-\mathbf{Q},\omega-\Omega)$ and combined with the local irreducible vertex [33] we obtain the full non-local spin and charge susceptibilities $\chi^{m,d}(\mathbf{Q},\Omega)$. The susceptibilities are computed on a $16\times16\times16$ $\mathbf{Q}$-mesh. BSE equations in the particle-particle pairing channels are solved on the same k-mesh to extract the susceptibilities and the Eliashberg eigenvalue equations are solved to extract the eigenvalue spectrum and corresponding pairing symmetries [36].

Author contributions

SA has conceived and designed the research. SA, DP, MvS have carried out the calculations. SA, DP, HP, MvS have contributed codes. DP, MvS have prepared the figures. All authors have contributed to the writing of the paper and the analysis of the data.

Additional information

Supplementary material is available.

Competing financial interests

The authors declare no competing financial interests.

Correspondence

All correspondence, code and data requests should be made to SA.

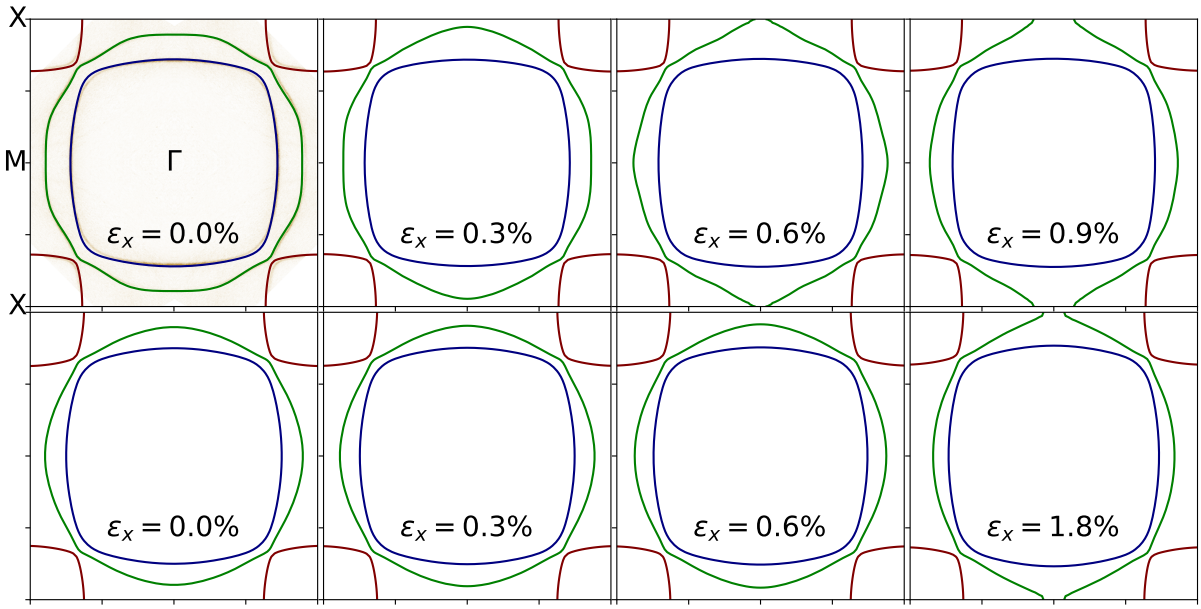

Figure 1: **Evolution of Fermi surface topology under strain:** Top row shows the QS*GW* Fermi surfaces in the basal plane, for a [100] compressive strain with ϵ_x=(0%, 0.3%, 0.6%, 0.9%). Spin orbit coupling is included (its omission makes a modest change to the Fermi surfaces). In the first panel (top left) high-resolution ARPES data [28] (figure is replotted using the raw ARPES data) for the Fermi surfaces are shown (figure reproduced with due permission) in the background of our QS*GW* theoretical data. For a higher resolution comparison please see the SM. States derive almost exclusively of Ru t_{2g} orbitals xy, xz, yz; the orbital character of each pocket changes moving around the contour. xy character is present on the entire Fermi surface: it resides on the blue pocket on the Γ-X line, and on the green on the Γ-M line. Under strain, the four M points lose the 4-fold rotational symmetry, and at $\epsilon_x = \epsilon_x^*$ the topology of the green band changes. Bottom row shows corresponding results for DFT. In DFT the transition also occurs, but near ϵ_x=1.8% (bottom right panel), instead of ϵ_x^*.

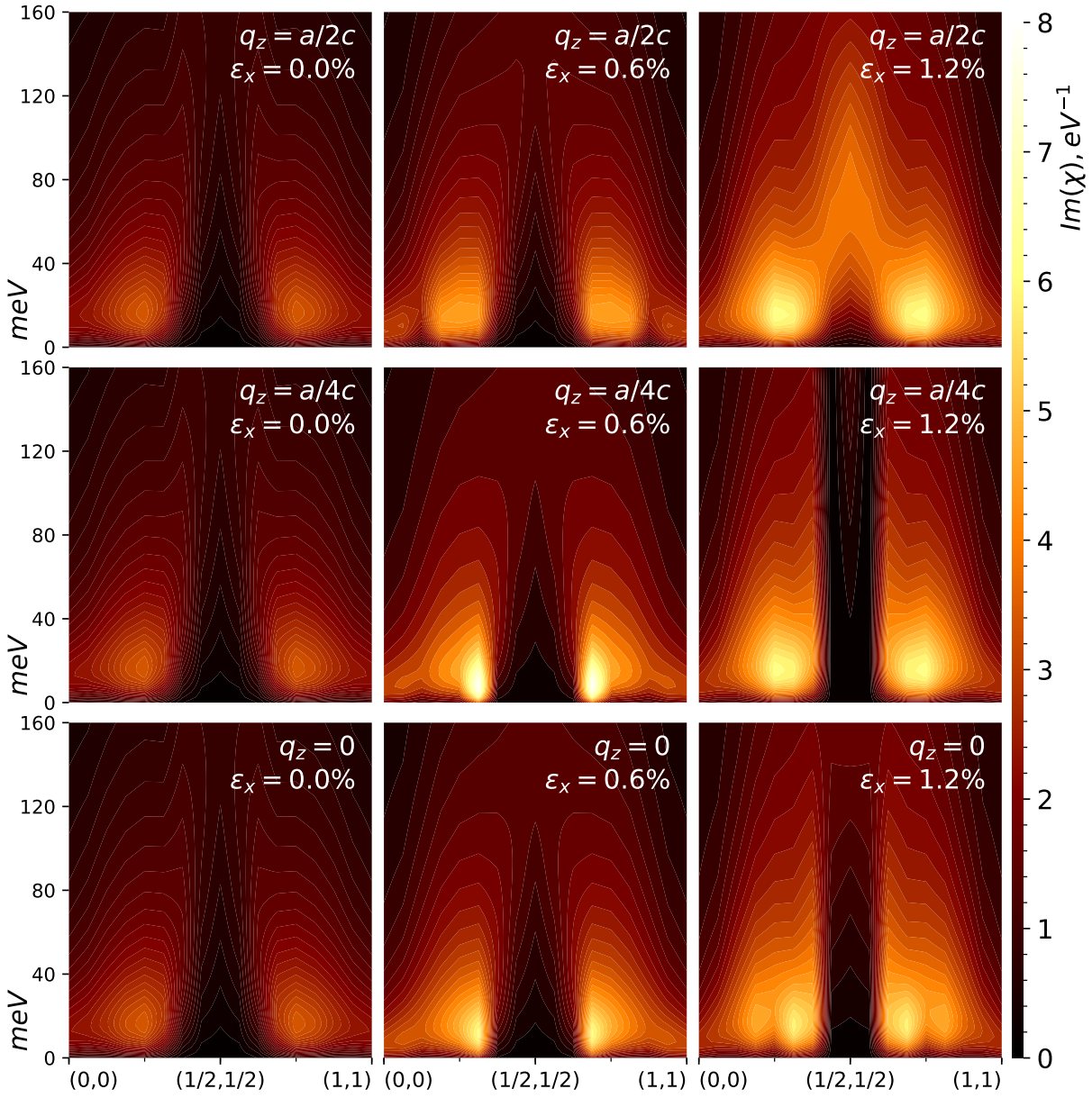

Figure 2: **Spin fluctuations: incommensurability and coherence:** Imaginary part of the dynamic spin susceptibility $\chi^m(q,\omega)$ are shown in the Cartesian xy plane at different values q_z, and for different strains ϵ_x. The unstrained compound shows a spin fluctuation spectrum strongly peaked at $(0.3, 0.3, q_z)$ (units $2\pi/a$). At ϵ_x=0, χ^m is nearly independent of q_z, but it begins to depend on q_z for ϵ_x>0. With increasing strain fluctuations become more coherent and strongly peaked, reaching a zenith at ϵ_x=ϵ_x^* (0.6%), where T_c is maximum. For ϵ_x>ϵ_x^*, this peak becomes more diffuse; also a secondary incoherent peak emerges at $(0.15, 0.15, q_z)$, and the quasi anti-ferromagnetic vector $(1/2, 1/2, a/2c)$ acquires spectral weight around ω=40 meV. Note also the spectral weight near the FM vector (0,0,0), and its evolution with ϵ_x.

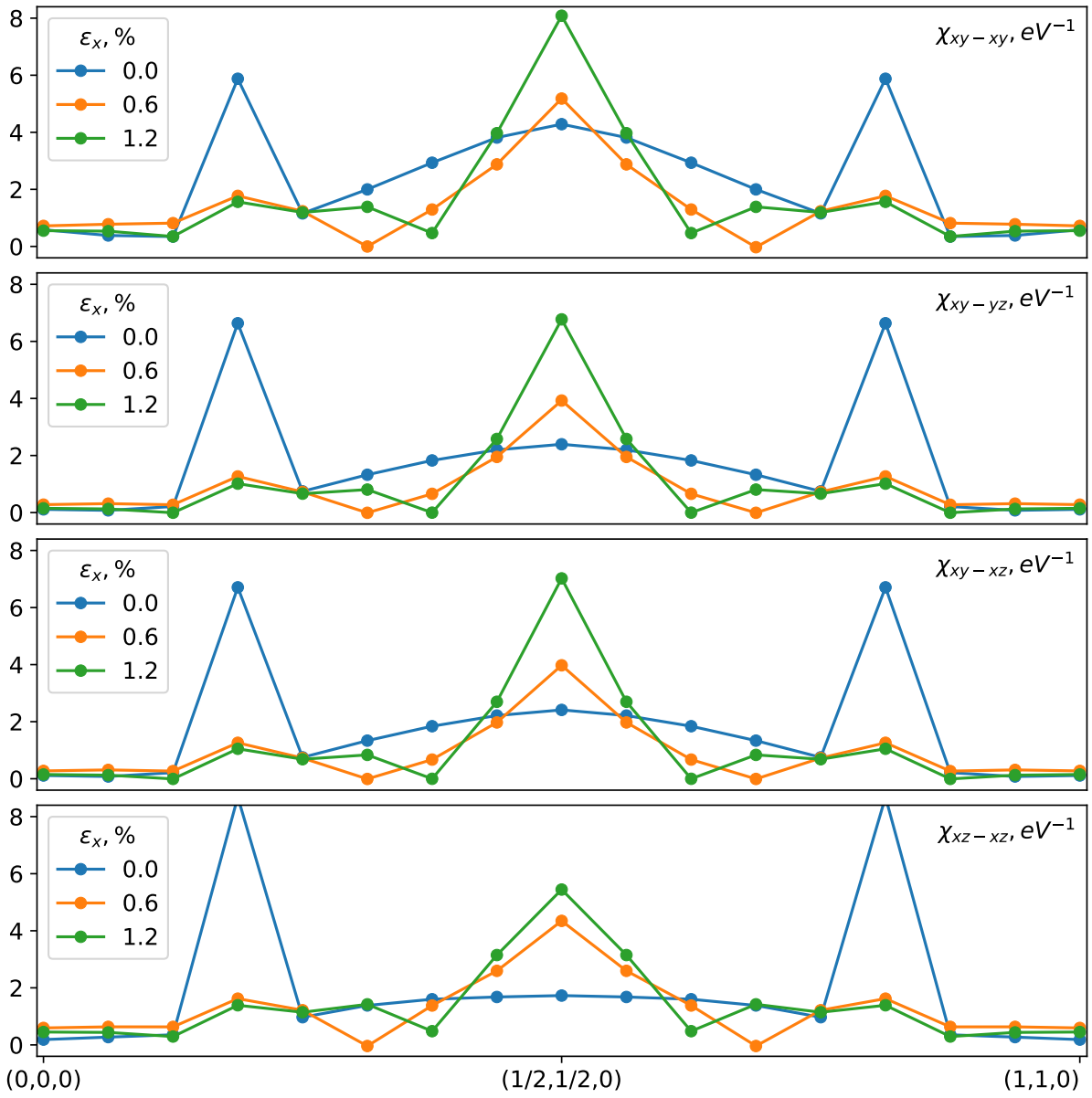

Figure 3: **Charge susceptibilities and commensurability:** Real part of the static charge susceptibility $\chi^d(q, \omega = 0)$, shown along the Cartesian (000) to (110) direction, and for different strains ϵ_x. The unstrained compound shows three-peaked charge fluctuation, with sharp peaks at IC vector (0.2, 0.2, 0) (and by symmetry at (0.8, 0.8, 0)) and a broad peak at (0.5, 0.5, 0). With strain the structure becomes sharply single-peaked at commensurate (0.5, 0.5, 0). The peak at the commensurate vector develops at the cost of the charge fluctuation weights from the IC vectors. The systematic evolution from large wavelength triplet to shorter wavelength singlet fluctuations, under strain, is common to all inter- and intra-orbital charge fluctuations. The strong, often the most dominant, inter-orbital charge fluctuations can be observed in Ru-d_{xy-xz} and Ru-$d_{xy,yz}$ channels.

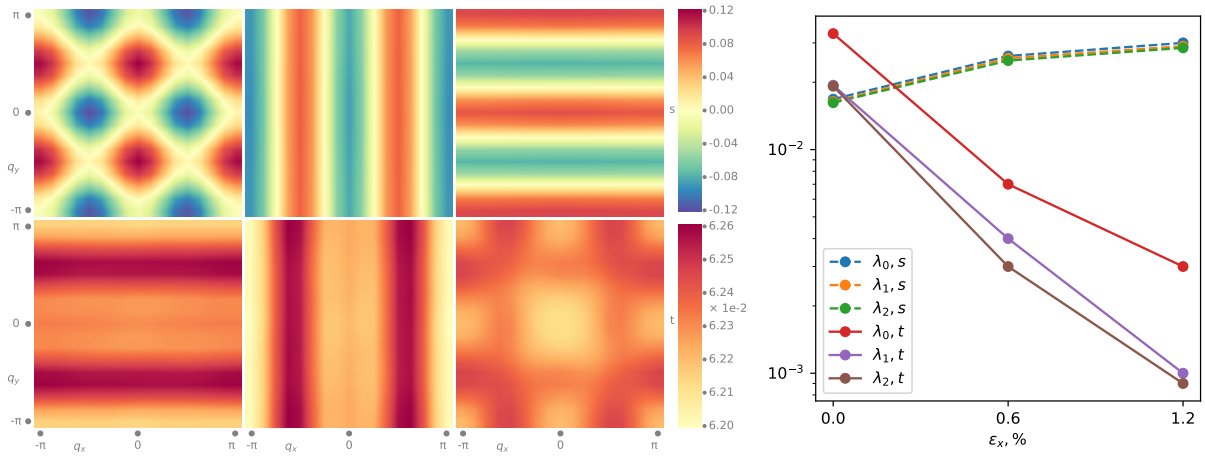

Figure 4: **Superconducting pairing functions and eigenvalues:** (left panel) The superconducting pairing gap symmetries for ϵ_x=0 are shown in the conventional basal plane; eigenfunctions corresponding to first three eigenvalues in singlet (s) symmetries are in the top panel and triplets (t) are in the lower panel . Right panel shows evolution of triplet and singlet eigenvalues (at 380 K) under strain. Under strain singlet eigenvalues increase and surpass the triplet eigenvalues.

References

[1] H. Onnes, *Commun. Phys. Lab. Univ. Leiden* (1911).

[2] L. N. Cooper, *Phys. Rev.* **104**, 1189 (1956).

[3] A. Mackenzie, *et al.*, *Physical review letters* **80**, 161 (1998).

[4] C. Nayak, S. H. Simon, A. Stern, M. Freedman, S. D. Sarma, *Reviews of Modern Physics* **80**, 1083 (2008).

[5] Y. Maeno, *et al.*, *Nature* **372**, 532 (1994).

[6] A. P. Mackenzie, T. Scaffidi, C. W. Hicks, Y. Maeno, *npj Quantum Materials* **2**, 40 (2017).

[7] Y. Maeno, *et al.*, *Physical review letters* **81**, 3765 (1998).

[8] S. Kittaka, T. Nakamura, H. Yaguchi, S. Yonezawa, Y. Maeno, *Journal of the Physical Society of Japan* **78**, 064703 (2009).

[9] Y. Ying, *et al.*, *Physical review letters* **103**, 247004 (2009).

[10] C. W. Hicks, *et al.*, *Science* **344**, 283 (2014).

[11] A. Steppke, *et al.*, *Science* **355**, eaaf9398 (2017).

[12] Y. Imai, M. Sigrist, *Physica B: Condensed Matter* **536**, 72 (2018).

[13] Y.-C. Liu, F.-C. Zhang, T. M. Rice, Q.-H. Wang, *npj Quantum Materials* **2**, 12 (2017).

[14] M. E. Barber, A. S. Gibbs, Y. Maeno, A. P. Mackenzie, C. W. Hicks, *Physical review letters* **120**, 076602 (2018).

[15] J. Mravlje, *et al.*, *Physical review letters* **106**, 096401 (2011).

[16] C. Veenstra, *et al.*, *Physical review letters* **112**, 127002 (2014).

[17] S. Acharya, M. S. Laad, D. Dey, T. Maitra, A. Taraphder, *Scientific Reports* **7**, 43033 (2017).

[18] L. Boehnke, P. Werner, F. Lechermann, *arXiv preprint arXiv:1806.01511* (2018).

[19] G. Baskaran, *Physica B: Condensed Matter* **223**, 490 (1996).

[20] S. Acharya, D. Dey, T. Maitra, A. Taraphder, *Journal of Physics Communications* (2018).

[21] S. Acharya, *et al.*, *Phys. Rev. X* **8**, 021038 (2018).

[22] L. Sponza, *et al.*, *Physical Review B* **95**, 041112 (2017).

[23] J. M. Tomczak, M. van Schilfgaarde, G. Kotliar, *Phys. Rev. Lett.* **109**, 237010 (2012).

[24] D. Pashov, *et al.*, *arXiv preprint 1907.06021* (2019).

[25] Questaal website, https://www.questaal.org. Our GW implementation was adapted from the original ecalj package, now at https://github.com/tkotani/ecalj/.

[26] P. Steffens, *et al.*, *arXiv preprint arXiv:1808.05855* (2018).

[27] C. Bergemann, A. Mackenzie, S. Julian, D. Forsythe, E. Ohmichi, *advances in Physics* **52**, 639 (2003).

[28] A. Tamai, *et al.*, *Phys. Rev. X* **9**, 021048 (2019).

[29] S. Liu, *et al.*, *Physical Review B* **86**, 165112 (2012).

[30] M. Braden, *et al.*, *Physical Review B* **66**, 064522 (2002).

[31] M. Braden, *et al.*, *Physical review letters* **88**, 197002 (2002).

[32] K. Ishida, *et al.*, *Physical Review B* **63**, 060507 (2001).

[33] H. Park, K. Haule, G. Kotliar, *Phys Rev Lett.* **107**, 137007 (2011).

[34] K. Iida, *et al.*, *Physical Review B* **84**, 060402 (2011).

[35] S. Raghu, A. Kapitulnik, S. Kivelson, *Physical review letters* **105**, 136401 (2010).

[36] H. Park, The study of two-particle response functions in strongly correlated electron systems within the dynamical mean field theory, Ph.D. thesis, Rutgers University-Graduate School-New Brunswick (2011).

[37] Eigenfunctions displayed here are in the orbital basis of d states, and they are useful to distinguish intra- and inter-orbital character of the pairing. But to project the superconducting gap on the Fermi surfaces these functions must be recast into the basis of eigenfunctions. The momentum-dependent superconducting gap at the Fermi surface can be obtained by diagonalizing a Bogoliubov Hamiltonian constructed in the band basis. See Z. Yin, K. Haule, G. Kotliar, *Nature Physics* **10**, 845 (2014).

[38] K. Yishida, H. Mukuda, Y. Kitaoka, K. Asayama, Z. Q. Mao, Y. Mori, Y. Maeno Nature 396, 658 (1998).

[39] Jing Xia, Yoshiteru Maeno, Peter T. Beyersdorf, M. M. Fejer, and Aharon Kapitulnik, Phys. Rev. Lett. 97, 167002 (2006).

[40] G. M. Luke et al, Nature 394, 558 (1998).

[41] L.-D. Zhang, W. Huang, F. Yang, H. Yao, *Physical Review B* **97**, 060510 (2018).

[42] I. Eremin, D. Manske, S. Ovchinnikov, J. Annett, *Annalen der Physik* **13**, 149 (2004).

[43] G. Litak, J. Annett, B. Györffy, K. Wysokiński, *physica status solidi (b)* **241**, 983 (2004).

[44] P. Contreras, M. Walker, K. Samokhin, *Physical Review B* **70**, 184528 (2004).

[45] K. Ishida, *et al.*, *Phys. Rev. Lett.* **84**, 5387 (2000).

[46] M. Zhitomirsky, T. Rice, *Physical review letters* **87**, 057001 (2001).

[47] P. Contreras, M. Walker, K. Samokhin, *Physical Review B* **70**, 184528 (2004).

[48] A. Pustogow, *et al.*, *arXiv preprint arXiv:1904.00047* (2019).

[49] K. Ishida, M. Manago, Y. Maeno, *arXiv preprint arXiv:1907.12236* (2019).

[50] E. Hassinger, *et al.*, *Physical Review X* **7**, 011032 (2017).

[51] S. Kittaka, *et al.*, *Journal of the Physical Society of Japan* **87**, 093703 (2018).

[52] Gingras. Olivier *et al.*, arXiv preprint arXiv:1808.02527 (2018).

[53] T. Scaffidi, J. C. Romers, S. H. Simon, *Phys. Rev. B* **89**, 220510 (2014).

[54] L. Komendová, A. M. Black-Schaffer, *Phys. Rev. Lett.* **119**, 087001 (2017).

[55] K. Haule, G. Kotliar, *Phys. Rev. B* **76**, 104509 (2007).

[56] X. Deng, K. Haule, G. Kotliar, *Physical Review Letters* **116** (2016).

[57] Q. Huang,et al.,Journal of Solid State Chemistry112, 355 (1994)